Modeling the Relationship between the p53 C-Terminal Domain and Its Binding Partners Using Molecular Dynamics

William J. Allen,[†] Daniel G. S. Capelluto,[‡] Carla V. Finkielstein,[§] and David R. Bevan*[,†]

Department of Biochemistry, Virginia Polytechnic Institute and State University, 111 Engel Hall (0308), Blacksburg, Virginia 24061, United States and Protein Signaling Domains Laboratory and Integrated Cellular Responses Laboratory, Department of Biological Sciences, Virginia Polytechnic Institute and State University, 1981 Kraft Drive (0913), Blacksburg, Virginia 24061, United States

Received: February 5, 2010; Revised Manuscript Received: July 27, 2010

Fifty percent of all cancer cases result from mutations of the *TP53* gene, which encodes the tumor suppressor p53, and it is hypothesized that the p53-mediated checkpoint pathway is compromised in most of the remaining cases. The p53 C-terminal domain (CTD) is an important site of p53 regulation but by nature is difficult to study, as it is intrinsically disordered. In this study, we performed molecular dynamics simulations on the p53 CTD and five known regulatory binding partners. We identified distinct trends in fluctuation within and around the p53 CTD binding site on each partner demonstrating a behavior that facilitates association. Further, we present evidence that the size of the hydrophobic pocket in each p53 CTD binding site governs the secondary structure of the p53 CTD when in the bound state. This information will be useful for predicting new binding partners for the p53 CTD, identifying interacting regions within other known partners, and discovering inhibitors that provide additional points of control over p53 activity.

Downloaded via NATL UNIV OF SINGAPORE on September 30, 2018 at 04:05:02 (UTC).
See https://pubs.acs.org/sharingguidelines for options on how to legitimately share published articles.

Introduction

The p53 protein has been extensively studied since it was discovered and identified as an important tumor suppressor protein.[1] The p53 protein has the ability to promote cell cycle arrest, apoptosis, and antiangiogenesis among other functions, which it commonly does in aberrantly growing cells as a means to cease tumorigenisis.[2,3] Nonfunctioning p53, or a malfunction in the p53-mediated signaling pathway, results in tumor cell formation and abnormal proliferation. Most often, the defect is a single mutation within the *TP53* gene, but it can also result from altered expression or mutation of p53 regulatory proteins.[2] The general consensus remains that restoration of p53 function in a malignant cell is of tremendous therapeutic benefit.[4]

The p53 C-terminal domain (CTD) represents a widely accepted site for its regulation.[5,6] It is promiscuous in both function and activity, performing many roles in the cell. The p53 CTD binds DNA nonspecifically to promote linear diffusion along the DNA,[7,8] but it can also bind DNA in a more sequence-specific manner depending on its lysine acetylation state.[9,10] As a way to regulate this DNA-binding function, the p53 CTD also binds nonspecifically to RNA.[11] The p53 CTD also binds other proteins, some of which are transcription cofactors to be recruited to specific genes,[12−14] some sequester or block p53 activity by directly binding to the C-terminus,[15,16] and many others regulate p53 activity through post-translational modification (PTM).[17−20] The p53 CTD contains sites of methylation, acetylation, phosphorylation, and ubiquitination among others. The topic of PTM has been studied extensively and is well reviewed[4,21,22] and will not be further discussed here.

A key feature that makes the p53 CTD promiscuous is the fact that the entire domain (residues 363−393) is disordered.[23] Disordered proteins have several different functions, a major one being recognition and binding of various biomolecules.[24,25] The nature of being disordered gives disordered regions the distinct advantage of being able to bind nonspecifically to a multitude of different partners, in a sense becoming a "hub" of protein interaction.[26] This phenomenon assumes importance when the hub in question is at the center of a cancer-prevention pathway.[27]

The association of the p53 CTD to its various partners varies in specificity, type, and mode of binding. For example, when bound to S100 calcium-binding protein B (S100B($\beta\beta$)), the CTD forms an α-helix that spans residues 377−387 (PDB 1DT7),[28] but when it binds to a Sirtuin protein (Sir2), it forms a β-strand from residues 380 to 385 (PDB 1MA3).[29] In addition to these distinct secondary structure elements, the CTD forms a β-turn when bound to cAMP response element-binding (CREB) binding protein (CBP) (PDB 1JSP),[14] and it lacks any ordered secondary structure when bound to the histone methyltransferase Set9 (PDB 1XQH)[19] or the cyclin A/cyclin-dependent protein kinase 2 complex (PDB 1H26).[30] Thus, these five binding partners were chosen for this study for their diverse range of size, function, and nature of interaction with the p53 CTD, as well as for their structure availability.

Our knowledge of the binding process between the p53 CTD and its binding partners is limited. At present, there are two models under consideration: (i) the p53 CTD transiently forms the appropriate secondary structure in solution before binding to its partner,[31] or (ii) the p53 CTD adopts the appropriate secondary structure upon coming in close proximity to its binding partner, a process known as induced folding.[32,33] A recent study suggests that the p53 CTD is able to form α-helices transiently in solution, but in the case of binding to S100B($\beta\beta$), it only forms the secondary structure when induced by the binding partner.[34] This conformational diversity gives the p53

* To whom correspondence should be addressed. Phone: (540) 231-5040. Fax: (540) 231-9070. E-mail: drbevan@vt.edu.
[†] Department of Biochemistry.
[‡] Protein Signaling Domains Laboratory, Department of Biological Sciences.
[§] Integrated Cellular Responses Laboratory, Department of Biological Sciences.

10.1021/jp1011445 © 2010 American Chemical Society
Published on Web 09/27/2010

CTD the advantage of being a viable binding site for its partners at all times, instead of merely when it happens upon the correct configuration. To our knowledge, there is no other evidence, theoretical or physical, that describes the binding event between the p53 CTD and any of its partners other than S100B($\beta\beta$). This limitation makes it very difficult to predict novel protein partners for the p53 CTD as well as to identify their binding sites and the conformation that the p53 CTD adopts in the complex.

Molecular simulation is a useful technique to study disordered proteins and their interactions. The disordered N-terminus transactivation domain,[35−38] the structured DNA-binding domain,[39−43] and the tetramerization domain,[44] which is immediately N-terminal to the p53 CTD, have all been studied using molecular dynamics (MD) techniques. The p53 CTD has also been studied by molecular simulation to a limited extent. Namely, there are MD and docking studies on the interaction between p53 CTD and various small molecules in complex with S100B,[34,45,46] as well as MD and docking studies on the p53 CTD binding region on CREB binding protein.[47] Apart from these examples, no one has yet performed a rigorous MD study of the interaction between the p53 CTD and a broad spectrum of binding partners.

This report seeks to answer a few fundamental questions about the nature of the interaction between the p53 CTD and its binding partners. First, what features of the recognition sites within the binding partners promote association to the p53 CTD? Second, what is the nature of the interaction among those two molecules? Third, what effect does the binding event have on the structural dynamics of the p53 CTD and of its interacting protein? Better understanding of these relationships will help the prediction of putative binding sites on other partners or even in the identification of novel interacting proteins.

Computational Methods

PDB File Preparation. Five files were downloaded from the Research Collaboratory for Structural Bioinformatics Protein Data Bank (www.pdb.org).[48] Each contains two important elements: some fragment of the p53 CTD and some binding partner. In each structure file, an N-terminal acetyl cap and C-terminal amide cap were added to the p53 CTD fragment using the LEaP program in AMBER.[49] All crystallographic waters were removed. The following subsections provide specific information on further file preparation.

1DT7. This structure file contains 40 nuclear magnetic resonance (NMR) spectroscopy models of the interaction between the rat protein S100B($\beta\beta$) homodimer and a human p53 CTD 22-mer fragment (residues 367−388).[28] Of the 40 models, the first one was chosen for the simulations (structure validation is discussed in the Analysis section). In the chosen model, the C-terminal carboxyl group was missing from each chain of the S100B($\beta\beta$) homodimer, so it was rebuilt using LEaP. The other two chains in the NMR model (Chain X and Chain Y) are p53 CTD fragments, and each is bound to one of the S100B subunits. Chain X was also missing the C-terminal carboxyl group, so it was rebuilt in LEaP before the cap was added as described in the previous section. Chain Y was removed for simplicity, and the other three modified chains (S100B($\beta\beta$) homodimer and one p53 CTD chain) were considered for the final model. Because p53 CTD binding to S100B($\beta\beta$) is calcium dependent, all four calcium ions were also preserved.

1MA3. This crystal structure solved at 2.00 Å contains Sir2 in complex with a p53 CTD 9-mer fragment (residues 379−387).[29] Several residues of the Sir2 protein are missing, including a loop from residues 30 to 39 and residue 253; in addition, there are atoms missing from residues Glu 29, Arg 112, and Glu 252. In order to rebuild the loop and repair the other inaccuracies, we employed Modeller 9v4[50−53] using the complete protein sequence and the 1MA3 crystal structure as the template. We built 10 different conformations for the loop from residues 30 to 39 and scored the models within the SWISS-MODEL Workspace.[54] We chose the best scoring model and relied on the forthcoming MD simulations to further refine the loop.

In the crystallization experiment, an 18-mer fragment of the p53 CTD (residues 372−389) was used but only a 9-mer fragment (residues 379−387) was solved. The low electron density in the unsolved residues implies a large amount of flexibility and fluctuation. Avalos et al.[29] found that the essential interactions are the burying of AcLys 382 in a hydrophobic pocket and the formation of a β-sheet, both of which are conserved in our model. The Arg 379, however, was missing several atoms that were rebuilt in LEaP before adding on the caps as previously described. Further, residue Lys 382 of the p53 CTD is acetylated in the original structure. Finally, two other components had to be considered. First, a zinc ion coordinated by Sir2 was retained. Second, one molecule of 2-(*N*-morpholino)-ethanesulfonic acid that crystallized with the proteins as an artifact of the crystallization process was deleted.

1H26. This crystal structure solved at 2.24 Å resolution contains several important elements.[30] The foundation is formed by a complex of two proteins, cyclin A and phosphorylated cyclin-dependent protein kinase 2 (pCDK2), of which there are two copies in the crystallographic asymmetric unit. A p53 CTD 9-mer fragment (residues 378−386) is bound to one of the cyclin A chains. The cyclin A/pCDK2 pair that was not bound to the p53 CTD was deleted. The two most C-terminal residues of pCDK2 were missing most of their atoms, and because the location is well removed from the binding site with the p53 CTD, the remaining atoms were deleted and the chain was terminated after Leu 296 with a carboxyl group in LEaP.

1JSP. This structure file contains 20 NMR models of a p53 CTD 20-mer fragment (residues 367−386) in complex with the CREB binding protein (CBP) bromodomain.[14] The Lys 382 of the p53 CTD fragment is monoacetylated, a factor that is necessary for binding. The first of the 20 NMR structures was chosen for this study (structure validation is discussed in the Analysis section). No missing residues or atoms needed to be repaired or added other than the caps discussed previously.

1XQH. This crystal structure contains the methyltransferase Set9 in complex with a p53 CTD fragment solved at 1.75 Å resolution.[19] In the crystallization experiment, a 10-mer fragment (residues 369−378) of the p53 CTD was used but only a 6-mer fragment (residues 369−374) was resolved. The crystallographic asymmetric unit contained two copies of the protein complex, and one of the pairs was deleted for simplicity. The N-terminal 14 residues of Set9 were also not distinguished by crystallography but are located far enough from the p53 CTD binding site that they were not rebuilt. Finally, Lys 372 of the p53 CTD was monomethylated in the original crystal structure.

Molecular Dynamics Simulations. In total, 15 systems were prepared for simulation. For each of the five PDB files, we simulated (i) the complex of the p53 CTD fragment and binding partner prepared as described in the previous sections, (ii) the p53 CTD fragment alone, and (iii) the binding partner alone. The initial coordinates of simulation groups (ii) and (iii) were taken directly from group (i). All MD simulations were performed with GROMACS 4.0.4[55] in conjunction with the

united atom GROMOS 53a6 force field.[56] Methylated and acetylated lysine parameters were reasonably adapted by combining existing parameters in the 53a6 force field and are included in the Supporting Information (Tables S1−S3 and Figure S1). The systems were solvated using the explicit simple point charge (SPC) water model,[57] and enough sodium and chloride ions were added to neutralize the charge of each system and bring the final concentration to a physiological level of 100 mM. Each system was then energy minimized using a steepest descents integrator[58] either until the maximum force was less than 1000 kJ mol^{-1} nm^{-1} on any atom or until additional steps resulted in a potential energy change of less than 1 kJ mol^{-1}.

A 50 ps NVT equilibration was performed at 200 K with position restraints applied to all of the backbone atoms in order to relieve any bad contacts at the side chain−solvent interface. The Berendsen thermostat[59] was used with a temperature coupling time constant (τ_T) of 0.1 ps. All bond lengths were constrained using the linear constraint solver (LINCS) algorithm,[60] which allowed for a 2 fs time step. Long-range electrostatic interactions were approximated using the particle-mesh Ewald (PME) method[61,62] with a fourth-order spline interpolation and a 0.12 nm Fourier grid spacing.

After the initial equilibration, the position restraints were lifted and the Berendsen thermostat was raised to 310 K for a 100 ps NVT simulation. Once each system was sufficiently equilibrated around the target temperature, the Nosé−Hoover thermostat[63,64] was applied because it generates a more correct canonical distribution for temperature and simulated for another 100 ps (NVT) at the same temperature. Finally, a 100 ps NPT simulation was conducted, relaxing the system into an isotropic Parrinello−Rahman barostat[65,66] set to 1.0 bar of pressure in all directions and a pressure coupling time constant (τ_P) of 1.0 ps. The production MD that followed was performed with the Nosé−Hoover thermostat and Parrinello−Rahman barostat, as well as the LINCS and PME treatments as described.

Replicate systems were generated using the same starting configuration but with different initial velocities applied prior to the first NVT equilibration at 200 K. Each of the 15 simulations was simulated in triplicate for 100 ns, for a total simulation time of 4.5 μs across all simulations. Simulations were performed on Virginia Tech's System X Supercomputer, a 12.25 Teraflop computer comprising 1100 Apple PowerMac G5 computers with dual 2.3 GHz PowerPC 970FX processors.[67]

Analysis. All analyses were performed using the GROMACS suite of tools and a secondary structure recognition algorithm (DSSP).[68] The hydrophobic solvent-accessible surface area (SASA) of each p53 CTD binding site was determined by measuring the SASA of all hydrophobic residues that lie within the p53 CTD binding site and/or interact closely with the p53 CTD. All of the pertinent residues that were considered are listed in the Results and Discussion section. It is important to mention that a bug in the code for the GROMACS analysis tool *"g_rmsf"* was fixed as outlined on the GROMACS Web site prior to performing our analyses. The program Grace[69] was used to plot the 2-D data, and the 3-D images were created with either PyMOL[70] or Chimera.[71]

In order to verify that our simulation subspace overlaps completely with the NMR structural subspace, thus validating our choice in starting structure for 1DT7 and 1JSP, we employed methods outlined in the literature[72,73] (Figures S2 and S3 and Tables S4 and S5, Supporting Information). We found good overlap in the structural ensembles of the receptor proteins but less overlap in the p53 CTD conformations. In each NMR structure, the solvent-exposed portion of the CTD is disordered and observed to be in many different random solvent-oriented conformations. It is unlikely that traditional MD on this time scale could reproduce the solvent-exposed configurations in the NMR structure, but we are satisfied that the ensemble of structures at the p53 CTD−binding partner interface for each structure was satisfactorily sampled across the three replicates.

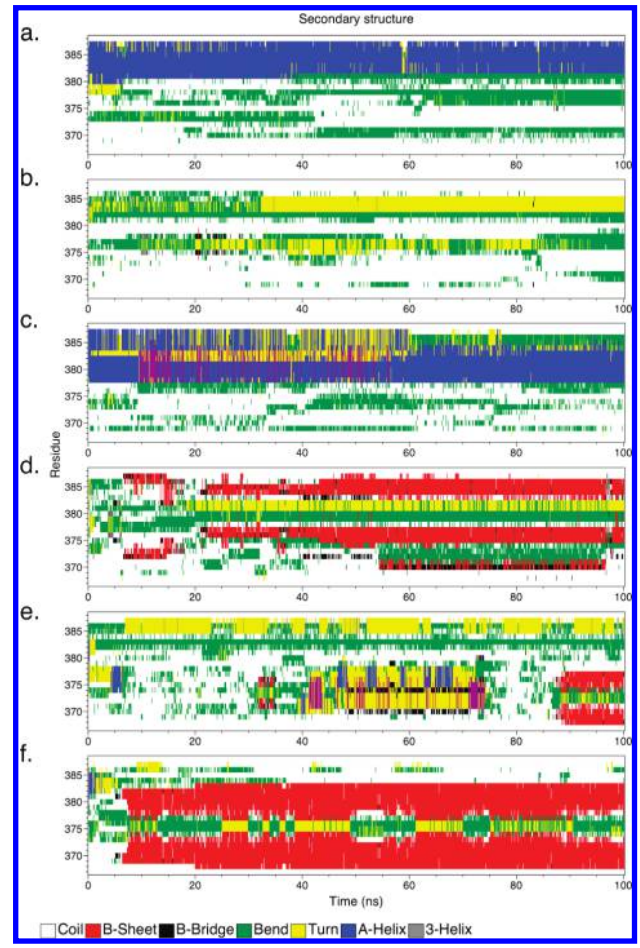

Figure 1. DSSP analysis for 1DT7. (a−c) Secondary structure content of the p53 CTD when bound to S100B($\beta\beta$). (d−f) Secondary structure content of the unbound p53 CTD.

Results and Discussion

In the following subsections, MD simulations will be discussed as follows. First, we will compare the dynamics of the p53 CTD fragment when bound to a binding partner or unbound in solution. Second, we will compare the dynamics of each binding partner when bound to the p53 CTD fragment and unbound in solution. Finally, we discuss specific interactions of interest for each p53 CTD−binding partner pair. Discussions are organized by the PDB identifier from which the structures originated.

1DT7. We first assessed the stability during MD of the p53 CTD fragment (residues 367−388) when bound to the S100B($\beta\beta$) receptor by analyzing the DSSP profile (Figure 1). When bound to the receptor, the p53 CTD underwent little change from the starting structure in all three replicates (Figure 1a−c). In the first and third replicates, the α-helix comprising residues 380−387 was well conserved. In the second replicate, the same helix unwound at the ends slightly and was calculated by the DSSP algorithm to be a turn, one residue short of being considered a true α-helix. When the p53 CTD was simulated unbound to the receptor from the same starting configuration,

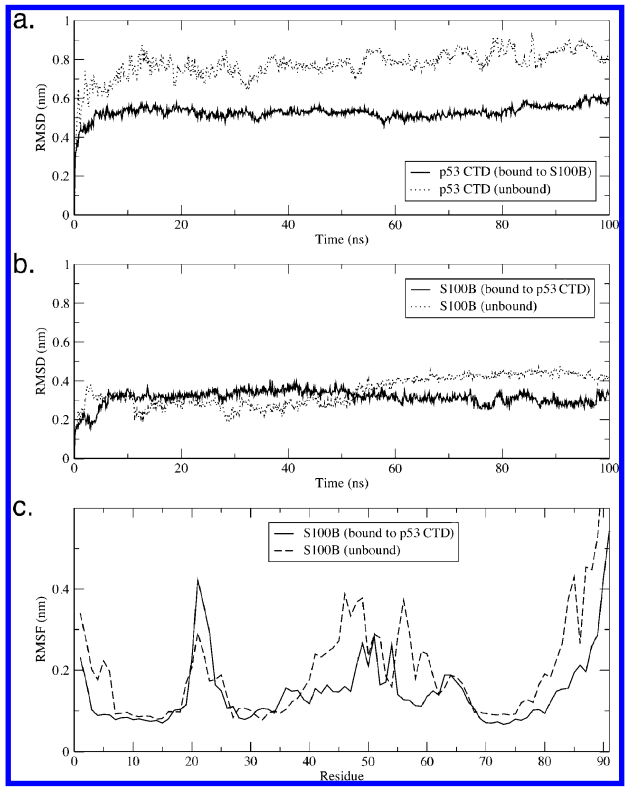

Figure 2. rmsd and RMSF analyses for 1DT7. (a) Average backbone rmsd for the three replicates of the p53 CTD in complex with S100B($\beta\beta$) (solid line) and in the absence of S100B($\beta\beta$) (dotted line). (b) Average backbone rmsd for the three replicates of the S100B($\beta\beta$) receptor in complex with the p53 CTD (solid line) and in the absence of the p53 CTD (dotted line). (c) RMSF of S100B($\beta\beta$) in complex with the p53 CTD (solid line) and in the absence of the p53 CTD (dashed line).

a major change in secondary structure content occurred that spanned all three replicates (Figure 1d−f). The peptide adopted many different secondary structure elements, most notably β-sheets, none of which retained any semblance to the original starting structure of the same peptide in complex with S100B($\beta\beta$).

The root-mean-square deviation (rmsd) of the p53 CTD also varied between bound and unbound states. Specifically, when the p53 CTD was bound to S100B($\beta\beta$), the average backbone rmsd of the three replicates was markedly lower than when the p53 CTD was unbound (Figure 2a). This evidence is in agreement with the DSSP evidence in that the p53 CTD fragment fluctuated less when bound to its receptor.

In the analysis of S100B($\beta\beta$), we find similar results. The average backbone rmsd of the three replicate simulations of S100B($\beta\beta$) bound to the p53 CTD was slightly lower than for the unbound form over the last 50 ns of simulation (Figure 2b). These data indicate that when in complex with the p53 CTD fragment, the S100B($\beta\beta$) receptor fluctuates less compared to when it is free in solution. It is also noteworthy that the rmsd of the bound form stabilized in less than 10 ns, whereas the rmsd of the unbound form stabilized in roughly 70 ns. A root-mean-square fluctuation (RMSF) analysis revealed specific parts of the protein that fluctuated more (or less) in the bound or unbound states (Figure 2c). The hinge region (residues 40−49), helix 3 (residues 50−60), and helix 4 (residues 70−88) of the S100B β-subunit comprise the p53 CTD binding site (Figure 3), and they all exhibited a higher degree of fluctuation when the p53 CTD was not bound. In contrast, residues important in calcium binding (residues 20−25) fluctuated more when the p53 CTD was bound.

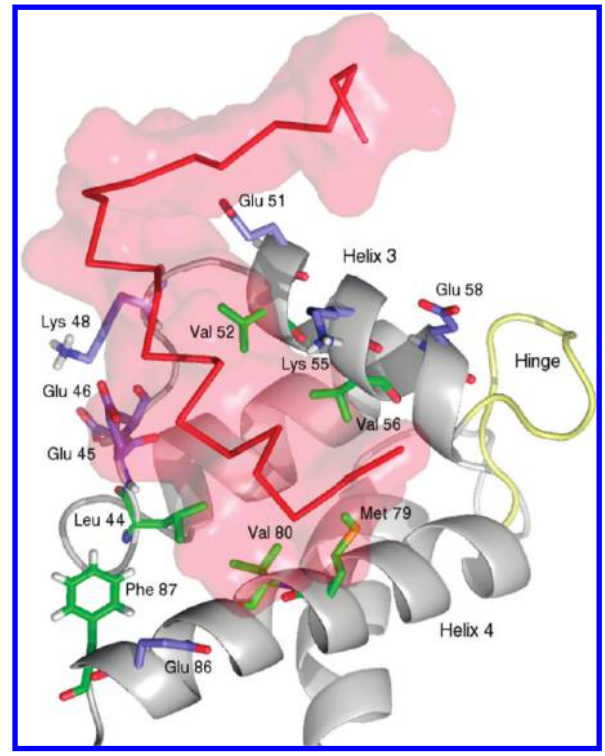

Figure 3. Surface rendering and backbone trace of the p53 CTD (red) bound to cartoon representation of one S100B β-subunit (gray). The hinge region is colored in yellow. Polar and acidic residues of the S100B β-subunit are represented with blue carbon atoms. Hydrophobic and aromatic residues are represented with green carbon atoms. Other atoms are colored according to standard schemes (H = white, O = red, N = dark blue, S = yellow).

The S100B β-subunit experienced a marked change in configurational principal components (PCs) upon p53 CTD binding. Briefly, PCs are eigenvectors that describe large collective (nontranslational and nonrotational) motions of atoms in a given protein that are observed over long time scales. PC vectors are determined in conjunction with a covariance matrix that illustrates correlated and anticorrelated motions of atoms. Figure 4a shows a covariance matrix for the two states of the S100B β-subunit, bound to the p53 CTD (bottom right) and in the absence of the p53 CTD (top left). When unbound, the S100B(β) subunit experienced large areas of both correlated and anticorrelated motion, specifically between helix 3 and helix 4, the helices that shape the p53 CTD binding site. In Figure 4b, the first principal component is illustrated as the beginning (top) and end (bottom) of its eigenvector. In the absence of the p53 CTD, a drastic transition in the shape of helix 3 and helix 4 and a change in relative position between the two helices is apparent from the two states, a transition which comprised 41.7% of the total motion in the protein. When the p53 CTD was bound, however, both correlated and anticorrelated motion dissipated between helix 3 and helix 4 (Figure 4a). The eigenvector that described the largest PC was a relatively small shift in the position of helix 3 (Figure 4b). Further, this PC represented only 25.5% of the total motion in the protein.

These data taken together, we observed a stabilization effect on the p53 CTD fragment upon binding to the receptor S100B($\beta\beta$), a characteristic that is in accordance with previous experimental observations.[28] Because these simulation conditions are consistent with experimental observations, we feel confident in making new observations about the dynamics of the receptor in both the bound and unbound state, as well as the interaction between the receptor and the p53 CTD fragment.

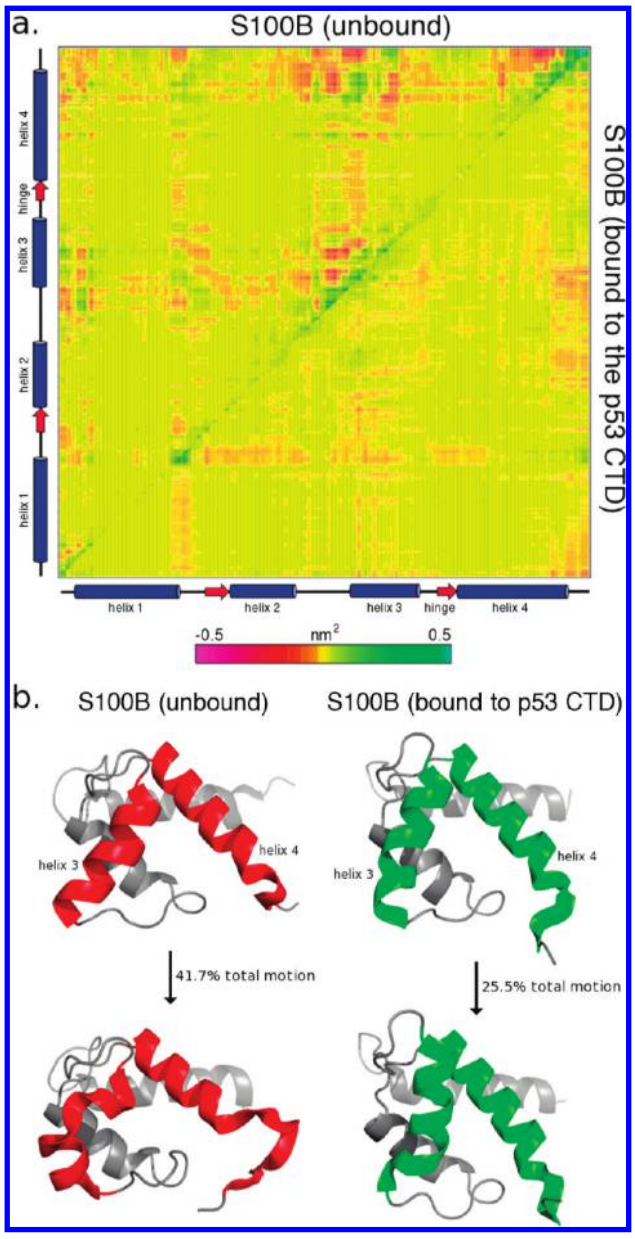

Figure 4. PC analysis for 1DT7. (a) Covariance matrix illustrating correlated and anticorrelated motions within one S100B β-subunit in the absence of the p53 CTD (top left) and when bound to the p53 CTD (bottom right). The secondary structure of the S100B β-subunit backbone is represented along the axes (from left to right, and from bottom to top). (b) Motion of the largest eigenvector on the S100B($\beta\beta$) structure in the absence of the p53 CTD (left) and when bound to the p53 CTD (right). The sites on S100B($\beta\beta$) where the p53 CTD binds are colored red and green.

The major contributing factors that stabilize the interaction between the p53 CTD and S100B($\beta\beta$) are summarized in Figure 5. Two important residues for this peptide−protein interaction are Arg 379 and Lys 382 of the p53 CTD, which exhibited large negative potential energies of interaction with the receptor. The residue Arg 379 formed persistent hydrogen bonds with His 42 and Glu 45 of S100B($\beta\beta$), whereas Lys 382 formed hydrogen bonds with Glu 86 and the backbone carbonyl oxygen of Phe 88. Residues His 368, Ser 378, and Lys 381 also formed many favorable electrostatic contacts with other S100B($\beta\beta$) residues, especially among those in helix 3 and helix 4, which exhibited a larger fluctuation in the apo-form of the protein, including residues Glu 45, Glu 46, Lys 48, Glu 49, Glu 51, Lys 55, and Glu 89. The Lys 386 residue of the p53 CTD also formed electrostatic interactions with Gln 71 and Glu 86 of the opposite β-subunit.

The van der Waals contacts formed by both Arg 379 and Lys 382 further contribute to the binding of the p53 CTD peptide to S100B($\beta\beta$). The hydrophobic binding pocket on S100B($\beta\beta$) is defined by residues Leu 44, Val 52, Val 56, Met 79, Val 80, and Phe 87. The average hydrophobic solvent-accessible surface area (SASA) of the binding site on S100B($\beta\beta$) was 3.18 ± 0.22 nm^2 over the last 50 ns of simulation (Figure 6). Residue Leu 383 of the p53 CTD faced invariably into this hydrophobic core and contributed the greatest negative van der Waals potential of interaction to the peptide−protein interaction (Figure 5 and Table S6, Supporting Information). Residues Met 384 and Phe 385 as well as the hydrophobic portion of several other p53 CTD side chains further contributed to the binding event.

One possible explanation for the specific conformation that the p53 CTD peptide adopts is that an α-helix enables alignment of the hydrophobic residues (Leu 383, Met 384, Phe 385) toward the hydrophobic binding site. This argument would be more convincing if there were additional hydrophobic residues further N- or C-terminus on the peptide that would also be aligned to the binding site only in an α-helical conformation. As it stands, a turn or even random coil could allow for three adjacent residues to be aligned such that they face the same binding site. Another explanation could have to do with the relative shortage of hydrogen bond donors or acceptors within the large hydrophobic core. Most side chain hydrogen bonds are satisfied by the surrounding ring of acidic and polar amino acids as well as by the solvent, but the large hydrophobic patch does not provide sufficient hydrogen bond donors or acceptors for the p53 CTD backbone (Figure 7). Adopting a helical conformation solves this problem, as intrachain backbone hydrogen bonds are readily formed.

The p53 N-terminal transactivation domain (TAD) is a good model for comparison of the intricate peptide−receptor relationship. In a series of recent publications, Dastidar et al.[74−76] showed that the MDM2-bound form of the p53 TAD is a helix dominated by van der Waals interactions. The authors suggest that the α-helix is formed so that three hydrophobic residues (Phe 19, Trp 23, and Leu 25) all face into the hydrophobic binding pocket. Further, they found that the initial complex formation is dominated by electrostatic interactions, much like Chen[34] proposes with the "fly-casting" mechanism.[77] This fits with our RMSF measurements that describe large fluctuations in acidic and polar residues around the p53 CTD binding site in the apo-form and increased fluctuations among the hydrophobic residues in the bound form of S100B($\beta\beta$) (Figure 2c).

One important observation relates to the role of Ser 376 and Thr 377 of the p53 CTD. Rustandi et al.[28] suggested that these two residues are buried against the face of S100B($\beta\beta$), effectively blocking phosphorylation at these sites. Although our simulations agreed that Thr 377 tended to stay buried, forming hydrogen bonds with residues Glu 45, Glu 46, and Glu 49, we found that a small conformational shift that happened fairly quickly in all three replicates caused Ser 376 to become solvent exposed. This is illustrated by the very small potential energy of interaction between Ser 376 and the receptor (Figure 5) and by the infrequency of formation of mainchain hydrogen bonds to the receptor (Figure 7). Steric hindrance could still be a factor in preventing phosphorylation of that residue given its low angle along the protein surface.

Another interesting feature of S100B($\beta\beta$) is the calcium-binding domain. In their investigation, Rustandi et al.[28] determined that calcium binding to each S100B β-subunit induces a

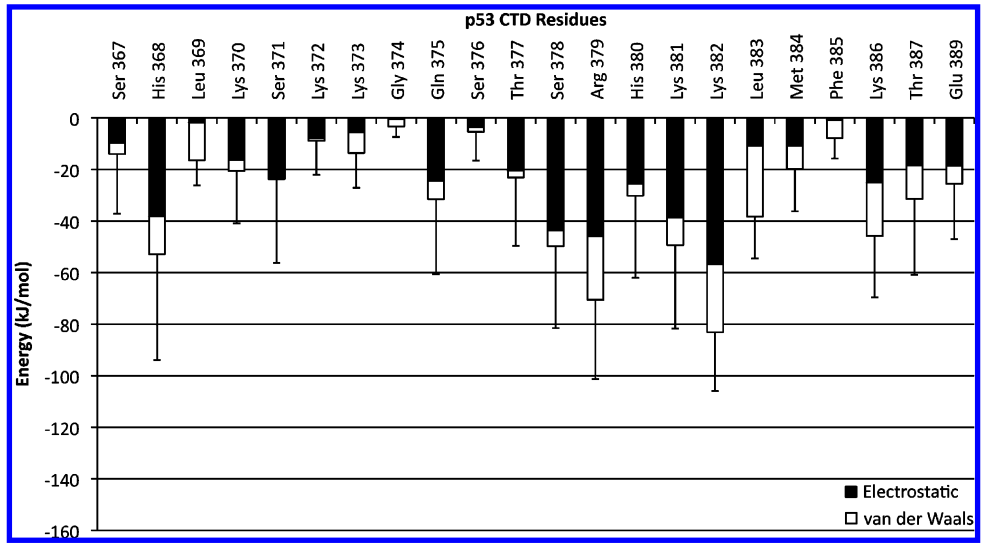

Figure 5. Potential energy of the interaction between the p53 CTD and S100B($\beta\beta$) by residue. The electrostatic contribution is shown in black, and the van der Waals contribution is shown in white. Error bars represent the standard deviation in the sum of the interactions.

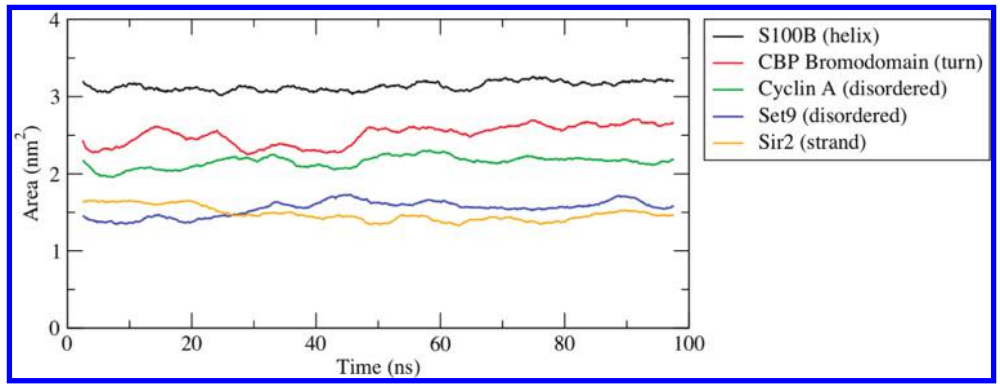

Figure 6. Hydrophobic SASA of the p53 CTD binding site on each apo-binding partner. The typical secondary structure content that the p53 CTD adopts when bound to each partner is listed in the legend in parentheses. The data presented are averaged over the three replicates of the apo-form of the binding partner and smoothed over a 20-point sliding window.

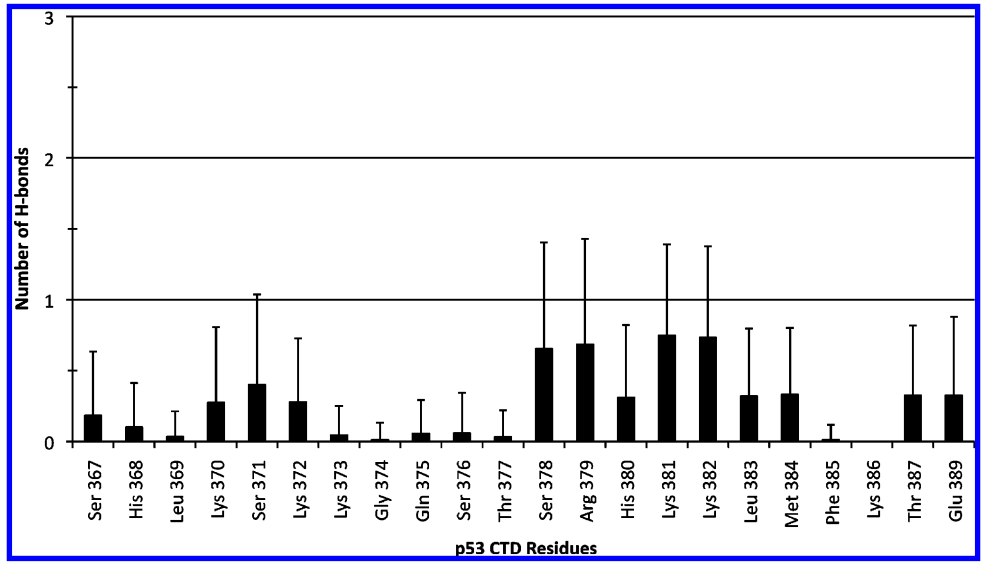

Figure 7. Average number of hydrogen bonds formed between the main chain of each p53 CTD residue and the receptor, S100B($\beta\beta$).

major conformational change in helix 3, which forms part of the p53 CTD binding site. This change helps open part of the large hydrophobic core, including S100B($\beta\beta$) residues Met 79, Val 80, Leu 44, and Val 56, which are necessary for p53 CTD binding, corroborating the importance of the hydrophobic binding site suggested by our MD simulations. Interestingly, the RMSF data show that fluctuation in the calcium-binding domain actually increased when the p53 CTD was bound. It has previously been demonstrated that this observed redistribution of fluctuation can be a mechanism of entropic stabilization of the protein complex[78] or as a means for the receptor to bind its substrate (p53 CTD) more tightly.

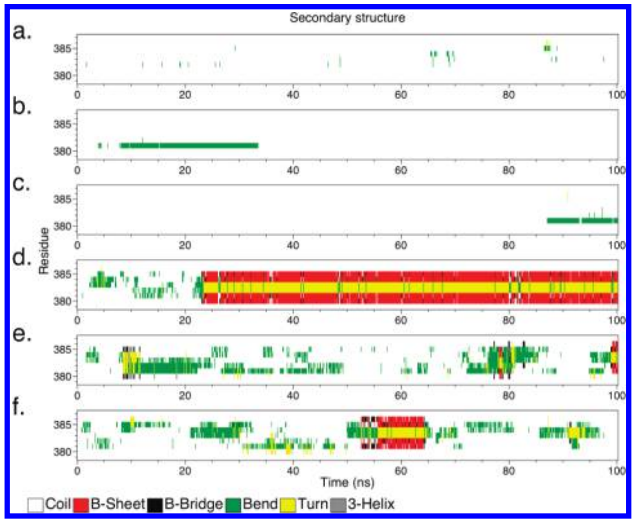

Figure 8. DSSP analysis for 1MA3. (a−c) Secondary structure content of the p53 CTD when bound to Sir2. (d−f) Secondary structure content of the unbound p53 CTD.

1MA3. In this crystal structure, the p53 CTD fragment (residues 379−387) is solved in complex with the deacetylase Sir2. From the DSSP profile (Figure 8), we observed that the p53 CTD fragment exhibited very little secondary structure content when bound to Sir2. The only notable structure formed was a turn centered at residue Lys 381, which only appeared with any consistency in two of the three replicates (Figure 8a−c). In the absence of Sir2, however, the same p53 CTD fragment adopted many different ordered conformations (Figure 8d−f), most notably a very short strand−turn−strand structure that persisted for almost 80 ns in one replicate and appeared for about 10 ns in another replicate. Concurrently, the rmsd analysis revealed an increase in average backbone deviation of the p53 CTD in the absence of Sir2 (Figure 9a). These data suggest that our MD simulations successfully reproduced the stabilization effect that Sir2 has on this p53 CTD fragment.[29]

In the analysis of Sir2, we found that a trend in backbone deviation was not as apparent as for the p53 CTD (Figure 9b). When the p53 CTD was not bound, the average backbone rmsd was only slightly higher than when the p53 CTD was bound. The RMSF analysis, however, clearly indicated two main regions that fluctuated more in the unbound form of the enzyme, residues 45−60 and residues 150−175 (Figure 9c). These stretches of amino acids include several regions that form the p53 CTD−Sir2 interface, including Glu 48, Glu 167, and Gln 171, as well as a short extension into the zinc-binding module of Sir2. This region includes the FGE loop (residues 162−169), which, when perturbed, opens up a binding tunnel that acts as a receptacle for AcLys 382 of the p53 CTD.[29] In contrast to the more flexible regions that existed in the unbound form of Sir2, there were a few regions that were more flexible in the p53 CTD-bound form of Sir2, most notably residues 69−77, 89−92, 106−112, 190−193, 206−211, and 219−225. Almost all of these regions are loops or helices that comprise the Rossman fold domain (residues 1−27, 77−118, and 170−253).

The largest PC (23.2%) in Sir2 while bound to the p53 CTD could be described as a pinching and releasing of the Rossman fold domain (Figure 10b). This motion corresponded nicely with an increased fluctuation in this region when bound to the p53 CTD. In contrast, the largest PC (29.4%) in the unbound form of Sir2 was a hinging motion at the p53 CTD binding site. This hinging motion is the same motion that was diminished by the formation of a β-sheet upon the p53 CTD binding. Figure 10a

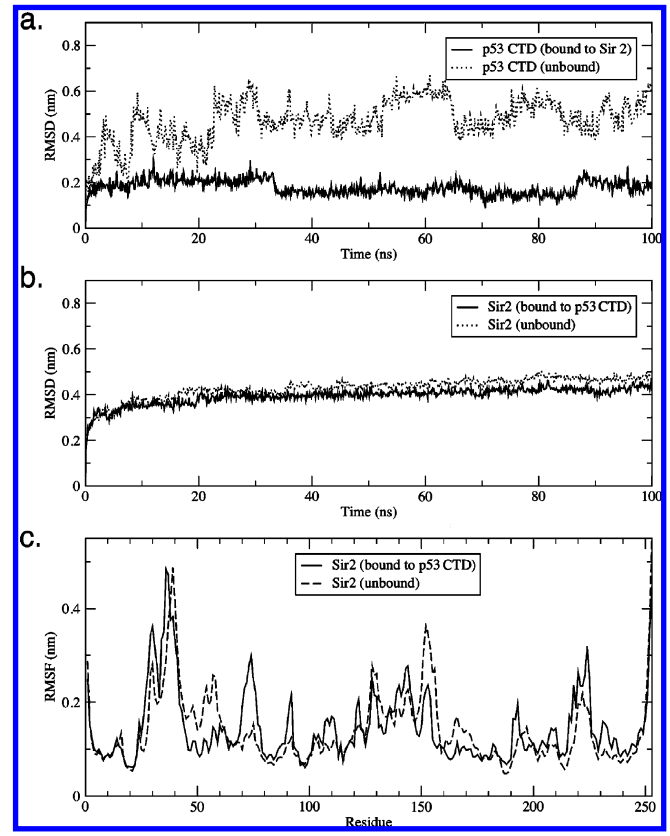

Figure 9. rmsd and RMSF analyses for 1MA3. (a) Average backbone rmsd for the three replicates of the p53 CTD in complex with Sir2 (solid line) and in the absence of Sir2 (dotted line). (b) Average backbone rmsd for the three replicates of the Sir2 receptor in complex with the p53 CTD (solid line) and in the absence of the p53 CTD (dotted line). (c) RMSF of Sir2 in complex with the p53 CTD (solid line) and in the absence of the p53 CTD (dashed line).

shows that there was a general increase in both correlated and anticorrelated motion across the entire Sir2 backbone when the p53 CTD was absent.

Here, we observed another instance in which hydrophilic and acidic residues near the hydrophobic binding site tended to fluctuate more in the apo-form of the receptor, presumably as a method to aid in the formation of initial contacts with the target.[76] Also, we detected another case in which the dynamics of a cofactor-binding site changed upon p53 CTD binding. The fluctuation and configurational dynamics (as calculated by the PC analysis) both increased in the NAD-binding domain when the p53 CTD was bound to Sir2. It is well established that increased fluctuations in active sites or cofactor-binding sites can be a means of induced catalysis.[79,80] These observations, therefore, are in accordance with the known biochemistry of the p53 CTD−Sir2 interaction in that the binding event leads to deacetylation of the peptide.[29]

One interesting observation regarding the p53 CTD−Sir2 interaction is that the stretch of the p53 CTD from residue 380 to 385 formed a β-strand when in complex with Sir2, while residues from that same stretch formed an α-helix when in complex with S100B($\beta\beta$) (although the DSSP algorithm did not identify the p53 CTD as a β-strand, the molecular geometry and the pattern of hydrogen bond formation was indicative of a β-strand). This β-strand joined two other β-strands of Sir2 (denoted β7 and β9, see Figure 11), forming a stable β-sheet. Avalos et al.[29] termed the role that the p53 CTD plays in this process as a "β-staple". One possible explanation for this observation is directly related to the proposed model of the

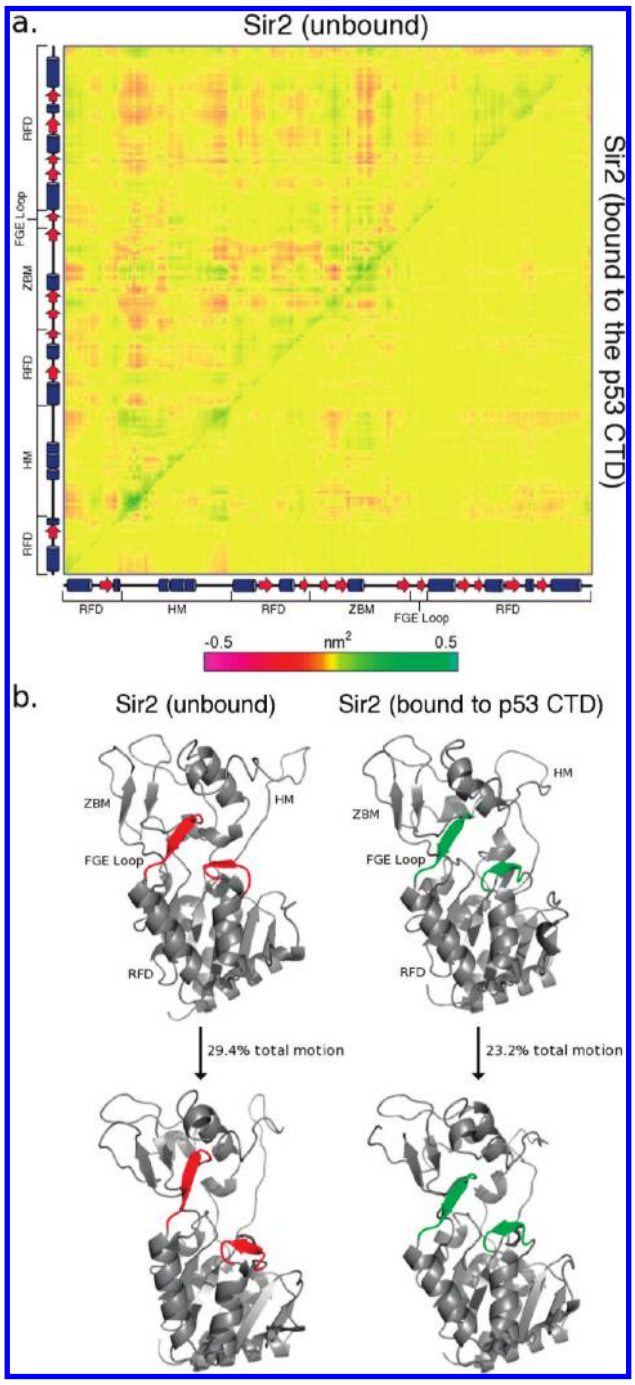

Figure 10. PC analysis for 1MA3. (a) Covariance matrix illustrating correlated and anticorrelated motions within Sir2 in the absence of the p53 CTD (top left) and when bound to the p53 CTD (bottom right). The secondary structure of the Sir2 backbone is represented along the axes (from left to right and from bottom to top). (b) Motion of the largest eigenvector on the Sir2 structure in the absence of the p53 CTD (left) and when bound to the p53 CTD (right). The sites on Sir2 that bind the p53 CTD are colored red and green.

formation of an α-helix in the p53 CTD upon binding S100B($\beta\beta$). In the case of Sir2, the hydrophobic SASA in the binding pocket is relatively small, measuring 1.43 ± 0.15 nm^2 averaged over the last 50 ns of simulation (Figure 6). An abundance of hydrogen bond donors and acceptors readily interact with the backbone of the p53 CTD (Figure 12), eliminating the need to form intrachain hydrogen bonds, as is the case in an α-helix.

The important interactions that maintained this β-sheet structure involved main chain and backbone hydrogen bonds

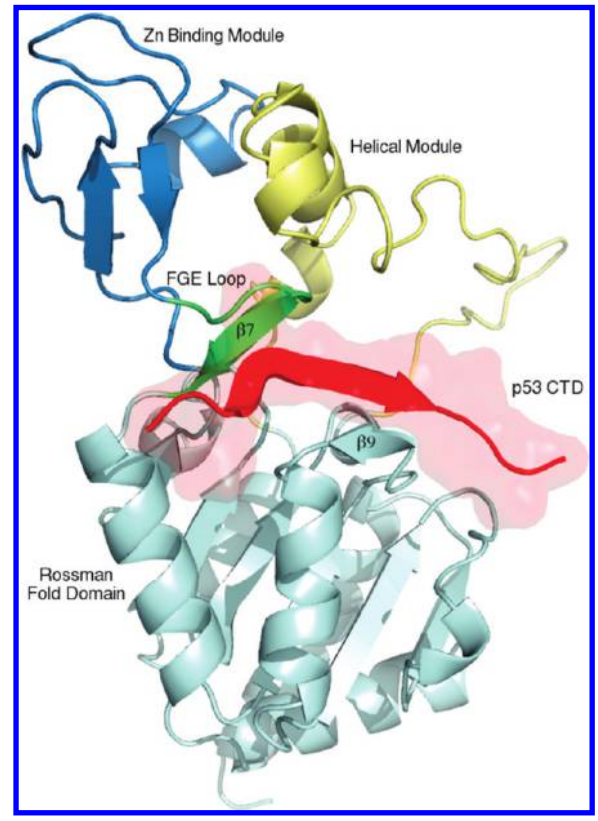

Figure 11. Cartoon representation of the p53 CTD (red) bound to Sir2. The Rossman fold domain is colored in cyan, the helical module is colored in yellow, the zinc binding module is colored in dark blue, and the FGE loop is colored in green. The two β-sheets (β7 and β9) with which the β-strand of the p53 CTD forms a β-staple are also labeled.

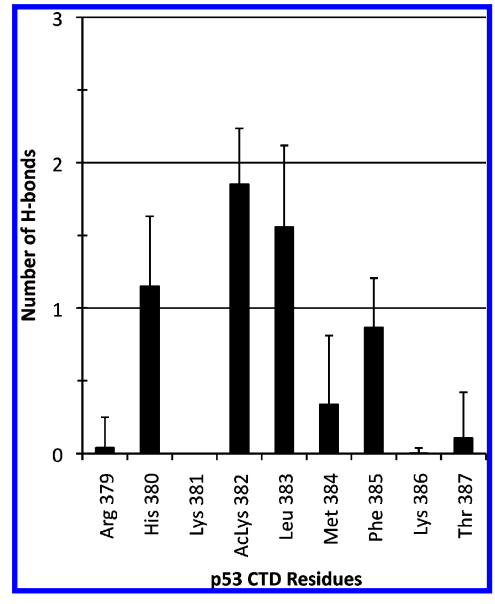

Figure 12. Average number of hydrogen bonds formed between the main chain of each p53 CTD residue and Sir2.

between highly conserved residues on the surface of Sir2.[29] For example, the main chain atoms of His 380 and AcLys 382 (p53 CTD) formed contacts with amino acids in the FGE loop of Sir2, Gly 166, Glu 167, and Leu 169. Further, the backbone atoms of Leu 383 and Phe 385 of the p53 CTD formed contacts with Val 195 and Tyr 197 of the Rossmann fold domain. We found that these contacts persisted in all three replicate simulations. However, the residue that contributed the largest negative

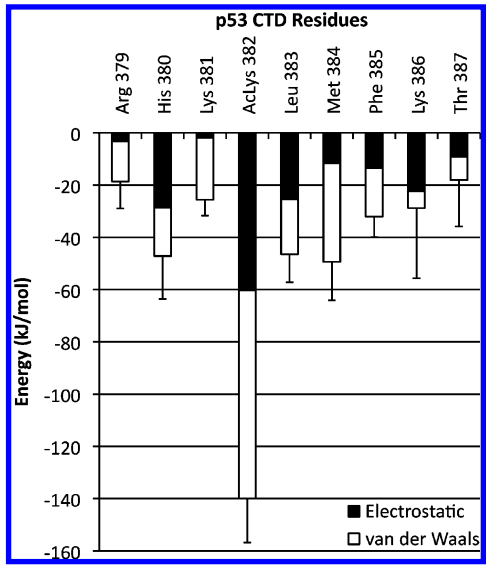

Figure 13. Potential energy of interaction between the p53 CTD and Sir2 by residue. The electrostatic contribution is shown in black, and the van der Waals contribution is shown in white. Error bars represent the standard deviation in the sum of the interactions.

potential energy of interaction was the AcLys 382 of the p53 CTD (Figure 13). The modified residue was buried deep within the hydrophobic pocket of the enzyme, a location that put it in proximity to the active site. Van der Waals interactions between AcLys 382 and several Sir2 residues (including His 118, Val 163, Phe 165, Leu 169, and Val 196) were the major contribution to the potential energy of interaction. In all three replicate simulations, the positioning of AcLys 382 remained unchanged.

1H26. Regarding the interaction between the p53 CTD and cyclin A, we began again by assessing the stability during MD of the p53 CTD fragment by measuring the DSSP profile (Figure S4, Supporting Information). In the three replicates in which the p53 CTD fragment was bound to cyclin A (Figure S4a−c, Supporting Information), nearly all of the secondary structure manifested as a bend or a turn centered around residue His 380. In some cases, the calculated secondary structure transitioned to coil during the simulation, and only very sparingly did any additional secondary structure other than coil appear within the p53 CTD fragment. In the three replicates in which the p53 CTD was not bound to its receptor (Figure S4d−f, Supporting Information), the appearance of random secondary structure was much more abundant and sporadic. Bend and turn elements appeared and disappeared between residues 380−384 with very little to no observable consistency.

When comparing the average backbone rmsd between the replicates (Figure S5a, Supporting Information), we found that the deviation in the p53 CTD fragment was slightly lower when it was in complex with the receptor, cyclin A. These data and the DSSP data together show that the bound form of the p53 CTD fragment was calculated to fluctuate less than the unbound form.

The dynamics of cyclin A appeared to change very little between the two states of the protein. The rmsd profile (Figure S5b, Supporting Information) shows an exceedingly slight increase in deviation between the bound and the unbound states. Similarly, a PC analysis did not reveal much change in the large-scale correlated motions in the protein upon p53 CTD binding. There was some increased motion in the loop immediately N-terminus to the α1 helix, as well as in both of the protein termini when the p53 CTD was not bound (Figure S6a, Supporting Information). Analysis of the greatest eigenvector in each system showed very little change in the actual p53 CTD binding site region (Figure S6b, Supporting Information). One possible explanation for this observation is that the p53 CTD fragment in question is only 9 amino acids in length, very small compared to the size of cyclin A (258 amino acids) and the size of the cyclin A-associated pCDK2 (297 amino acids) (Figure S7, Supporting Information). On this scale and in this time frame, it is difficult to measure any broad changes such as total backbone deviation.

Conveniently, we were able to measure local changes in the dynamics of the cyclin A receptor through a RMSF analysis (Figure S5c, Supporting Information). The RMSF analysis of cyclin A in both the p53 CTD-bound and the unbound states revealed two interesting features. First, a short stretch from residues 241 to 253 experienced a sharp increase in fluctuation upon p53 CTD binding. This stretch of residues gave shape to the core of the hydrophobic binding pocket and contains Leu 253, one of the cyclin A residues that interacted with the hydrophobic residues of the p53 CTD. Several other peaks in cyclin A that are also consistently high in RMSF across the replicates in which the p53 CTD fragment was bound are loops that surround the hydrophobic core (residues 194−207, 300−310, and 342−350). When the p53 CTD was not bound, the RMSF in cyclin A increased across residues 280−285, a loop that forms the outer ring of the binding pocket and encompasses Asp 283, a residue that is important in p53 CTD binding.

The p53 CTD binding site on cyclin A is characterized by a small hydrophobic binding pocket that averaged 2.20 ± 0.17 nm^2 of hydrophobic SASA over the last 50 ns of simulation (Figure 6). Residues Leu 383 and Phe 385 of the p53 CTD tended to form contacts in this pocket (which includes residues Ile 213, Leu 214, and Leu 253 of cyclin A), comprising the bulk of the van der Waals contribution to the potential energy of interaction (Figure S8, Supporting Information). In addition to these hydrophobic contacts, Ser 378, Arg 379, His 380, and Lys 381 of the p53 CTD formed recurring contacts with Glu 220, Glu 224, and Asp 283 of cyclin A, comprising a very large electrostatic potential of interaction (Figure S8, Supporting Information). Two frequently modified lysine residues of the p53 CTD (Lys 382 and Lys 386) tended to stay oriented toward the solvent in our simulations. It is noteworthy that the binding site in cyclin A has an abundance of readily available hydrogen bond donors and acceptors. These residues satisfied hydrogen bonds in the p53 CTD backbone, stabilizing the disordered conformation that the peptide maintained. Further, the hydrophobic pocket was much smaller in cyclin A than it was in S100B($\beta\beta$), and thus, there was less opportunity for the p53 CTD peptide to form intrachain backbone−backbone hydrogen bonds and consequently no tendency to form an α-helix structure.

The most interesting behavior seen in this binding pocket was the fluctuation pattern as measured by the RMSF analysis. Hydrophobic residues within the binding pocket increased in fluctuation upon p53 CTD binding, and polar and acidic residues near the entrance to the pocket increased in fluctuation when the p53 CTD was not bound. An explanation for this behavior is that when the p53 CTD bound to cyclin A, the hydrophobic residues from the p53 CTD effectively cap the hydrophobic pocket, creating a solvent-free hydrophobic cavity that the cyclin A residues may explore conformationally. When the p53 CTD was not bound, however, residues 280−285 of cyclin A increased in fluctuation. This increase may serve a dual purpose. First, one of these residues, Asp 283, represents another example

of an acidic residue that increased in fluctuation in the apo-form of the receptor to favor p53 CTD binding. Second, an increased fluctuation in this region partially conceals the hydrophobic binding site from the solvent, helping to preclude exposure to water molecules.

Overall, our data agree with interactions that have been previously described within the crystal structure of the complex.[30] Residues Leu 383 and Phe 385 of the p53 CTD are important residues for establishing hydrophobic contacts within the hydrophobic binding pocket, whereas Arg 379, His 380, and Lys 381 mediate important electrostatic interactions that occur between the p53 CTD and cyclin A.

1JSP. The DSSP profile of the p53 CTD taken from crystal structure 1JSP was very revealing (Figure S9, Supporting Information). In the three replicate simulations in which the p53 CTD was bound to the CBP bromodomain, we observed a moderate change in secondary structure content over the course of the MD simulations (Figure S9a−c, Supporting Information). The peptide fragment was typically characterized by turn or bend conformations along the middle of the chain. In the three replicate simulations of the p53 CTD fragment in the absence of the CBP bromodomain, drastic changes occurred (Figure S9d−f, Supporting Information). The first 10−20 ns of simulation progressed similarly to the receptor-bound replicates, but as the simulations passed the 20 ns mark, the N- and C-terminal ends of the p53 CTD fragment came together as β-strands to form an antiparallel β-sheet. This conformation was very stable and persisted for the rest of the simulation.

The rmsd analysis of the same p53 CTD fragment (Figure S10a, Supporting Information) showed that the average backbone deviation for the three replicates in which the peptide was not bound to the receptor was substantially higher than the same rmsd measurement for the three receptor-bound replicates. The secondary structure and rmsd analysis illustrated a considerable change in the structural features of the p53 CTD fragment in the absence of the CBP bromodomain.

The average backbone rmsd of the CBP bromodomain, however, actually increased in the presence of the p53 CTD (Figure S10b, Supporting Information), which is the only case in all five systems in which this phenomenon was observed. The RMSF analysis showed that the ZA loop (residues 1115−1138) of the CBP bromodomain fluctuated more when the p53 CTD was not bound (Figure S10c, Supporting Information). This loop contains several polar and acidic residues (including Asp 1124 and Asp 1127) that were oriented toward the solvent. Two loop regions increased in fluctuation once the p53 CTD was bound. These include the BC loop (residues 1170−1190) and a short strand−turn−strand structure that is just to the C-terminal side of the ZA loop (residues 1102−1112). Both of these loops flank the hydrophobic binding pocket (Figure S11, Supporting Information).

On a larger scale, a PC analysis showed that in the absence of the p53 CTD, the major eigenvector in the CBP bromodomain consisted of an opening and closing of the hydrophobic binding site between the ZA loop and the BC loop (Figure S12b, Supporting Information). This motion described 58.4% of the total motion in the protein. When the p53 CTD was bound, however, the same motion was dampened and dropped to only 23.8% of the total motion in the protein. From Figure S12a, Supporting Information, it is evident that upon p53 CTD binding there was a marked increase in both correlated and anticorrelated motion in the CBP bromodomain, especially among the ZA loop, the BC loop, and both of the termini. This observation is in agreement with the marked increase in rmsd that was observed in the CBP bromodomain backbone upon p53 CTD binding.

This case presents another example in which polar or acidic residues near the hydrophobic binding site tend to fluctuate more in the absence of the p53 CTD. This increase in fluctuation in the ZA loop is likely to assist in forming initial electrostatic contacts with the target peptide as observed in the interaction of MDM2 and the p53 TAD.[76] Further, we again observed a case in which hydrophobic residues that shape the binding site increased in fluctuation upon p53 CTD binding. This likely happens because p53 CTD binding effectively caps the binding site such that hydrophobic residues within the site are no longer constrained to avoid water contact and are free to explore a new hydrophobe-friendly conformational space. The PC analysis further confirms this hypothesis because of the observed increase in motion in the hydrophobic binding site upon p53 CTD binding (Figure S12, Supporting Information).

This molecular system is different from the other four structures considered in this study in that the contact area between the p53 CTD fragment (residues 367−386) and the CBP bromodomain (residues 1081−1196) in the NMR structure is limited to only a few residues. Of the 20-mer p53 fragment, the N-terminal 14 residues (367−380) are pointing away from CBP and exposed to the solvent and the C-terminal six residues (381−386) are in close contact with CBP. However, during the simulations, these N-terminal residues of the p53 CTD fragment folded over and formed contacts with the surface of the CBP bromodomain in as quickly as 2 ns and within 11 ns across all of the replicates. Specifically, polar residues along the p53 CTD backbone (His 368, Ser 371, Lys 373, Gln 375) interacted with Asp 1124 and Asp 1127 of the CBP bromodomain, depending on how the p53 CTD peptide folded during the simulation (Figure S13, Supporting Information). This shift in the p53 CTD conformation may have induced slight conformational changes along the backbone of the receptor that would not occur in the absence of the peptide, accounting for the increase in rmsd.

Another key interaction between the p53 CTD and the CBP bromodomain is the location of the AcLys 382 residue. This modified amino acid consistently remained inserted into the hydrophobic cavity in the CBP bromodomain formed by Val 1115, Ile 1122, Tyr 1125, Tyr 1167, Val 1174, and Phe 1177. The two residues to the C-terminal side of the acetylated lysine (Leu 383 and Met 384) also contributed to the negative potential energy of interaction within this pocket, while Phe 385 and Lys 386 formed contacts with the hydrophobic portion of Arg 1112 (Figure S13, Supporting Information). These hydrophobic contacts remained consistent across all three replicate simulations, indicating that they are likely the major contributing factor in the formation of the p53 CTD−CBP bromodomain complex. We measured the hydrophobic SASA in the binding site to be 2.61 ± 0.19 nm^2 over the last 50 ns of simulation (Figure 6). This area falls closer to that which supports helix formation rather than strand formation, which seems appropriate because the p53 CTD forms a turn structure when bound to the CBP bromodomain, one residue short of an α-helix.

1XQH. According to the DSSP analysis, when the p53 CTD was bound to the methyltransferase Set9, the only secondary structure detected was a bend centered at Ser 371 (Figure S14a−c, Supporting Information). Ser 371 formed a bend in all three replicates. The secondary structure content of the same fragment consistently changed in the absence of Set9 (Figure S14d−f, Supporting Information), forming sporadic turn and bend conformations across residues 370−374.

The average backbone rmsd of the same p53 CTD fragment was slightly higher when it was unbound compared to when it was bound early in the simulation, although they are comparable for the last 50 ns (Figure S15a, Supporting Information). These data, along with the DSSP analysis, demonstrate that the fluctuation in the p53 CTD fragment was lower when it was bound to the receptor Set9.

The average rmsd of the Set9 backbone was dependent on whether the p53 CTD fragment was bound (Figure S15b, Supporting Information). In the uncomplexed form, the average backbone deviation was slightly higher than in the bound form. A RMSF analysis identified three interesting regions within Set9 (Figure S15c, Supporting Information). When the p53 CTD was not bound, residues 252−266, a stretch that includes Asp 256 and Thr 266 (residues important in p53 CTD binding), increased in fluctuation. When the p53 CTD was bound, however, two different loops increased in fluctuation. These included residues 217−227 of the Set domain and 278−288 of the Set-I domain, both of which help the formation of the hydrophobic binding pocket in which the methylated Lys 372 of the p53 CTD was inserted (Figure S16, Supporting Information).

The PC analysis shows a very drastic difference in the dynamics of Set9 between the bound and unbound forms. When the p53 CTD was unbound, a single vector described 72.0% of the total motion in Set9. That vector corresponded to an opening and closing of the p53 CTD binding site region, or the area between the Set domain and the Set-I domain, through the major shift of the C-terminal segment (Figure S17b, Supporting Information). When the p53 CTD was bound, the same motion remained the largest PC but dropped to only a 38.3% contribution to overall motion in the protein. The major eigenvector revealed a much smaller shift of the C-terminal segment between the Set and Set-I domains (Figure 17b, Supporting Information). Figure S17a, Supporting Information, supports these observations, as it shows a general increase in motion in Set9 when it was not bound to the p53 CTD. Much of this motion could be described by fluctuations in the N- and C-terminus flanking domains, which settled upon p53 CTD binding.

Again, we observed hydrophilic and acidic residues (Asp 256 and Thr 266) with an increased fluctuation near the entrance to the hydrophobic binding site in the absence of the p53 CTD. The PC analysis also described an increased motion in these residues in the absence of the p53 CTD, indicating a propensity to form initial electrostatic contacts with its target, facilitating binding. Further, upon binding of the p53 CTD to Set9, we observed increased fluctuation in loops that form both the hydrophobic binding pocket and the cofactor (AdoHcy) binding site. Presumably, residues from the p53 CTD complete the shape of the pocket upon binding in a way that allows hydrophobic residues within the pocket to explore more conformational space (as previously described) and, in addition, promote methylation via induced catalysis.[79,80]

Chuikov et al.[19] solved the crystal structure of a p53 CTD fragment in complex with methyltransferase Set9. Originally, a 10-mer fragment of the CTD was used in the experiment (residues 369−378), but only the first six residues were well resolved (residues 369−374). Residue Lys 372 of the p53 CTD is methylated, a PTM that regulates p53 by restricting it to the nucleus.[19] In our simulations, we found that the MeLys 372 packed against Trp 260 of Set9, as it laid in a channel partly formed by the hydrophobic residues Val 255, Leu 267, and Val 158, with a hydrophobic SASA of roughly 1.60 ± 0.16 nm^2 (Figure 6). It also formed transient hydrogen bonds with Asn 265, Tyr 335, and Tyr 337, adding a substantial electrostatic potential energy contribution to the interaction (Figure S18, Supporting Information). Chuikov et al. proposed that this methylated lysine residue packs hydrophobically against Trp 260, but also they proposed that it forms hydrogen bonds with Arg 258 of Set9, for which we found no evidence in any of our three replicates.

In addition to the interactions of the methylated Lys 372, we found that residues Asp 256, Thr 266, and Ser 268 of Set9 formed stabilizing hydrogen bonds with several backbone atoms of the p53 CTD fragment, as well as with Ser 371 and Lys 373 of the p53 CTD. Chuikov et al.[19] suggested Arg 258 of Set9 as an important residue in p53 CTD binding, but we found that this residue tended to orient itself toward the solvent, away from the p53 CTD in all three replicates.

Conclusions

We studied the dynamics and interactions of five known p53 CTD-binding partner complexes by MD simulations. We looked for trends in the interactions and conformational dynamics that could be generalized and used to predict new binding partners for the p53 CTD or locate binding sites on already known partners for which there is no structural information related to protein−protein interactions.

We observed several important trends in the binding partners. Most importantly, the core of each p53 CTD binding site on the partners is a hydrophobic binding pocket that is variable in size. Further, these hydrophobic pockets typically increased in fluctuation upon binding of the p53 CTD. We propose that the binding event completes a cavity from which water is excluded, thereby allowing hydrophobic residues in the receptor to explore more conformational space. In addition, binding sites are typically surrounded by polar and acidic residues, which fluctuate more when the p53 CTD is not bound. This increased fluctuation suggests that the receptors facilitate p53 CTD binding by forming initial electrostatic contacts with the target peptide, as shown previously for the p53 TAD.[76] The complex, however, tends to rely heavily on van der Waals type contacts, especially within the hydrophobic cavity, for stabilization. Finally, in the case of receptors that also had a cofactor-binding site, we typically observed an increase in fluctuation at those sites upon p53 CTD binding. This is likely a mechanism to induce catalysis[79,80] or bind the peptide more tightly by entropic stabilization.[78]

We also propose a correlation between the size of the hydrophobic binding site and the secondary structure that the p53 CTD adopts upon binding. The p53 CTD has been observed to be an α-helix, a turn, a β-strand, or unstructured when in complex with a binding partner. We believe that the larger the hydrophobic area on the receptor, the p53 CTD will have a greater tendency to form a helix. This is due to the lack of hydrogen bond donors in the hydrophobic area. The backbone of the p53 CTD will have unsatisfied hydrogen bonds, thus favoring a helix conformation, which forms intrachain backbone−backbone hydrogen bonds. If the receptor has a very small hydrophobic area, we anticipate that the p53 CTD will favor a β-strand structure. The availability of hydrogen bond acceptors will be able to satisfy p53 backbone hydrogen bond donors. Receptors with medium-sized hydrophobic patches will induce unstructured or random coil structures on the p53 CTD backbone.

Overall, this information could be useful in designing inhibitors for p53 CTD−binding partner interactions. We would suggest exploiting the mechanism of binding facilitation of the polar and acidic amino acids near the binding site while keeping

in mind with careful consideration the size of the hydrophobic patch and its implication on the structure of the inhibitor. Further, this report will be useful to those trying to determine new binding sites for the p53 CTD among novel partners.

Acknowledgment. The authors thank Justin Lemkul for useful discussions about the methods and results of this project. Also, we thank the administrators of the Terascale Computing Facility at Virginia Tech for technical support and computing hours. This work was supported by the Institute for Critical Technology and Applied Science (ICTAS) at Virginia Tech.

Supporting Information Available: Additional tables, figures, and legends, including all analyses for sections 1H26, 1JSP, and 1XQH of the Results and Discussion. This material is available free of charge via the Internet at http://pubs.acs.org.

References and Notes

(1) Levine, A. J.; Finlay, C. A.; Hinds, P. W. P53 is a Tumor Suppressor Gene. *Cell* **2004**, *116*, S67–S69.

(2) Vogelstein, B.; Lane, D.; Levine, A. J. Surfing the p53 Network. *Nature* **2000**, *408*, 307–310.

(3) El-Deiry, W. S. Regulation of p53 Downstream Genes. *Semin. Cancer Biol.* **1998**, *8*, 345–357.

(4) Joerger, A. C.; Fersht, A. R. Structural Biology of the Tumor Suppressor p53. *Annu. Rev. Biochem.* **2008**, *77*, 557–582.

(5) Harms, K. L.; Chen, X. The C Terminus of p53 Family Proteins Is a Cell Fate Determinant. *Mol. Cell. Biol.* **2005**, *25*, 2014–2030.

(6) Kim, A. L.; Raffo, A. J.; Brandt-Rauf, P. W.; Pincus, M. R.; Monaco, R.; Abarzua, P.; Fine, R. L. Conformation and Molecular Basis for Induction of Apoptosis by a p53 C-terminal Peptide in Human Cancer Cells. *J. Biol. Chem.* **1999**, *274*, 34924–34931.

(7) McKinney, K.; Mattia, M.; Gottifredi, V.; Prives, C. p53 Linear Diffusion along DNA Requires Its C Terminus. *Mol. Cell* **2004**, *16*, 413–424.

(8) Tafvizi, A.; Huang, F.; Leith, J. S.; Fersht, A. R.; Mirny, L. A.; van Oijen, A. M. Tumor Suppressor p53 Slides on DNA with Low Friction and High Stability. *Biophys. J.* **2008**, *95*, L01–L03.

(9) Luo, J.; Li, M.; Tang, Y.; Laskowska, M.; Roeder, R. G.; Gu, W. Acetylation of p53 Augments its Site-Specific DNA Binding Both *in Vitro* and *in Vivo*. *Proc. Natl. Acad. Sci. U.S.A.* **2004**, *101*, 2259–2264.

(10) Friedler, A.; Veprintsev, D. B.; Freund, S. M. V.; von Glos, K. I.; Fersht, A. R. Modulation of Binding of DNA to the C-Terminal Domain of p53 by Acetylation. *Structure* **2005**, *13*, 629–636.

(11) Riley, K. J.-L.; Ramirez-Alvarado, M.; Maher, L. J., III. RNA-p53 Interactions in Vitro. *Biochemistry* **2007**, *46*, 2480–2487.

(12) Gu, W.; Shi, X.-L.; Roeder, R. G. Synergistic Activation of Transcription by CBP and p53. *Nature* **1997**, *387*, 819–823.

(13) Espinosa, J. M.; Emerson, B. M. Transcriptional Regulation by p53 through Intrinsic DNA/Chromatin Binding and Site-Directed Cofactor Recruitment. *Mol. Cell* **2001**, *8*, 57–69.

(14) Mujtaba, S.; He, Y.; Zeng, L.; Yan, S.; Plotnikova, O.; Sachchidan-and; Sanchez, R.; Zeleznik-Le, N. J.; Ronai, Z. e.; Zhou, M.-M. Structural Mechanism of the Bromodomain of the Coactivator CBP in p53 Transcriptional Activation. *Mol. Cell* **2004**, *13*, 251–263.

(15) Fernandez-Fernandez, M. R.; Veprintsev, D. B.; Fersht, A. R. Proteins of the S100 Family Regulate the Oligomerization of p53 Tumor Suppressor. *Proc. Natl. Acad. Sci. U.S.A.* **2005**, *102*, 4735–4740.

(16) Fernandez-Fernandez, M. R.; Rutherford, T. J.; Fersht, A. R. Members of the S100 Family Bind p53 in Two Distinct Ways. *Protein Sci.* **2008**, *17*, 1663–1670.

(17) Gu, W.; Roeder, R. G. Activation of p53 Sequence-Specific DNA Binding by Acetylation of the p53 C-Terminal Domain. *Cell* **1997**, *90*, 595–606.

(18) Chernov, M. V.; Bean, L. J. H.; Lerner, N.; Stark, G. R. Regulation of Ubiquitination and Degradation of p53 in Unstressed Cells through C-terminal Phosphorylation. *J. Biol. Chem.* **2001**, *276*, 31819–31824.

(19) Chuikov, S.; Kurash, J. K.; Wilson, J. R.; Xiao, B.; Justin, N.; Ivanov, G. S.; McKinney, K.; Tempst, P.; Prives, C.; Gamblin, S. J.; Bariev, N. A.; Reinberg, D. Regulation of p53 Activity through Lysine Methylation. *Nature* **2004**, *432*, 353–360.

(20) Feng, L.; Lin, T.; Uranishi, H.; Gu, W.; Xu, Y. Functional Analysis of the Roles of Posttranslational Modifications at the p53 C Terminus in Regulating p53 Stability and Activity. *Mol. Cell. Biol.* **2005**, *25*, 5389–5395.

(21) Bode, A. M.; Dong, Z. Post-Translational Modification of p53 in Tumorigenesis. *Nat. Rev. Cancer* **2004**, *4*, 793–805.

(22) Lavin, M. F.; Gueven, N. The Complexity of p53 Stabilization and Activation. *Cell Death Differ.* **2006**, *13*, 941–950.

(23) Bell, S.; Klein, C.; Müller, L.; Hansen, S.; Buchner, J. p53 Contains Large Unstructured Regions in its Native State. *J. Mol. Biol.* **2002**, *322*, 917–927.

(24) Tompa, P. The Interplay between Structure and Function in Intrinsically Unstructured Proteins. *FEBS Lett.* **2005**, *579*, 3346–3354.

(25) Dyson, H. J.; Wright, P. E. Intrinsically Unstructured Proteins and Their Functions. *Nat. Rev. Mol. Cell Biol.* **2005**, *6*, 197–208.

(26) Dunker, A. K.; Cortese, M. S.; Romero, P.; Iakoucheva, L. M.; Uversky, V. N. Flexible Nets. The roles of Intrinsic Disorder in Protein Interaction Networks. *FEBS J.* **2005**, *272*, 5129–5148.

(27) Iakoucheva, L. M.; Brown, C. J.; Lawson, J. D.; Obradovic, Z.; Dunker, A. K. Intrinsic Disorder in Cell-signaling and Cancer-associated Proteins. *J. Mol. Biol.* **2002**, *323*, 573–584.

(28) Rustandi, R. R.; Baldisseri, D. M.; Weber, D. J. Structure of the Negative Regulatory Domain of p53 Bound to S100B($\beta\beta$). *Nat. Struct. Biol.* **2000**, *7*, 570–575.

(29) Avalos, J. L.; Celic, I.; Muhammad, S.; Cosgrove, M. S.; Boeke, J. D.; Wolberger, C. Structure of a Sir2 Enzyme Bound to an Acetylated p53 Peptide. *Mol. Cell* **2002**, *10*, 523–535.

(30) Lowe, E. D.; Tews, I.; Cheng, K. Y.; Brown, N. R.; Gul, S.; Noble, M. E. M.; Gamblin, S. J.; Johnson, L. N. Specificity Determinants of Recruitment Peptides Bound to Phospho-CDK2/Cyclin A. *Biochemistry* **2002**, *41*, 15625–15634.

(31) Fuxreiter, M.; Simon, I.; Friedrich, P.; Tompa, P. Preformed Structural Elements Feature in Partner Recognition by Intrinsically Unstructured Proteins. *J. Mol. Biol.* **2004**, *338*, 1015–1026.

(32) Receveur-Bréchot, V.; Bourhis, J.-M.; Uversky, V. N.; Canard, B.; Longhi, S. Assessing Protein Disorder and Induced Folding. *Proteins* **2006**, *62*, 24–45.

(33) Dyson, H. J.; Wright, P. E. Coupling of Folding and Binding for Unstructured Proteins. *Curr. Opin. Struct. Biol.* **2002**, *12*, 54–60.

(34) Chen, J. Intrinsically Disordered p53 Extreme C-Terminus Binds to S100B($\beta\beta$) through Fly-Casting. *J. Am. Chem. Soc.* **2009**, *131*, 2088–2089.

(35) Lowry, D. F.; Stancik, A.; Shrestha, R. M.; Daughdrill, G. W. Modeling the Accessible Conformations of the Intrinsically Unstructured Transactivation Domain of p53. *Proteins* **2008**, *71*, 587–598.

(36) Espinoza-Fonseca, L. M. Leucine-rich Hydrophobic Clusters Promote Folding of the N-terminus of the Intrinsically Disordered Transactivation Domain of p53. *FEBS Lett.* **2009**, *583*, 556–560.

(37) Taranta, M.; Bizzarri, A. R.; Cannistraro, S. Modeling the Interaction Between the N-terminal Domain of the Tumor Suppressor p53 and Azurin. *J. Mol. Recognit.* **2009**, *22*, 215–222.

(38) Michel, J.; Harker, E. A.; Tirado-Rives, J.; Jorgensen, W. L.; Schepartz, A. In Silico Improvement of β3-Peptide Inhibitors of p53·hDM2 and p53·hDMX. *J. Am. Chem. Soc.* **2009**, *131*, 6356–6357.

(39) Lu, Q.; Tan, Y.-H.; Luo, R. Molecular Dynamics Simulations of p53 DNA-Binding Domain. *J. Phys. Chem. B* **2007**, *111*, 11538–11545.

(40) De Grandis, V.; Bizzarri, A. R.; Cannistraro, S. Docking Study and Free Energy Simulation of the Complex Between p53 DNA-binding Domain and Azurin. *J. Mol. Recognit.* **2007**, *20*, 215–226.

(41) Tomoda, K.; Takahashi, N.; Hibi, Y.; Asamitsu, K.; Ishida, H.; Kondo, T.; Yoshitaka, F.; Okamato, T. Molecular Docking Analysis of the Protein-protein Interaction between RelA-associated Inhibitor and the Tumor Suppressor Protein p53 and its Inhibitory Effect on p53 Action. *Cancer Sci.* **2008**, *99*, 615–622.

(42) Madhumalar, A.; Jun, L. H.; Lane, D. P.; Verma, C. S. Dimerization of the Core Domain of the p53 Family. *Cell Cycle* **2009**, *8*, 137–148.

(43) Khalili, M.; Wales, D. J. Computer Simulations of Peptides from the p53 DNA Binding Domain. *J. Chem. Theory Comput.* **2009**, *5*, 1380–1392.

(44) Lwin, T. Z.; Durant, J. J.; Bashford, D. A Fluid Salt-bridging Cluster and the Stabilization of p53. *J. Mol. Biol.* **2007**, *373*, 1334–1347.

(45) Gieldon, A.; Mori, M.; Del Conte, R. Theoretical Study on Binding of S100B Protein. *J. Mol. Model.* **2007**, *13*, 1123–1131.

(46) Withlow, J. L.; Varughese, J. F.; Zhou, Z.; Bartolotti, L. J.; Li, Y. Computational Screening and Design of S100B Ligand to Block S100B-p53 Interaction. *J. Mol. Graph. Model.* **2009**, *27*, 969–977.

(47) Sachchidanand; Resnick-Silverman, L.; Yan, S.; Mutjaba, S.; Liu, W.-j.; Zeng, L.; Manfredi, J. J.; Zhou, M.-M. Target Structure-Based Discovery of Small Molecules that Block Human p53 and CREB Binding Protein Association. *Chem. Biol.* **2006**, *13*, 81–90.

(48) Berman, H. M.; Westbrook, J.; Feng, Z.; Gilliland, G.; Bhat, T. N.; Weissig, H.; Shindyalov, I. N.; Bourne, P. E. The Protein Data Bank. *Nucleic Acids Res.* **2000**, *28*, 235–242.

(49) Case, D. A.; Darden, T. A.; Cheatham III, T. E.; Simmerling, C. L.; Wang, J.; Duke, R. E.; Luo, R.; Crowley, M.; Walker, R. C.; Zhang, W.; Merz, K. M.; Wang, B.; Hayik, S.; Roitberg, A.; Seabra, G.; Kolossváry, I.; Wong, K. F.; Paesani, F.; Vanicek, J.; Wu, X.; Brozell, S. R.; Steinbrecher, T.; Gohlke, H.; Yang, L.; Tan, C.; Mongan, J.; Hornak, V.;

Cui, G.; Mathews, D. H.; Seetin, M. G.; Sagui, C.; Babin, V.; Kollman, P. A. *AMBER 10*; University of California: San Francisco, 2008.

(50) Eswar, N.; Marti-Renom, M.-A.; Webb, B.; Madhusudhan, M. S.; Eramian, D.; Shen, M.; Pieper, U.; Sali, A. Comparative Protein Structure Modeling With MODELLER. In *Current Protocols in Bioinformatics*; John Wiley & Sons, Inc.: New York, 2006; Vol. Suppl. *15*, pp5.6.1−5.6.30.

(51) Sali, A.; Blundell, T. L. Comparative Protein Modelling by Satisfaction of Spatial Restraints. *J. Mol. Biol.* **1993**, *234*, 779–815.

(52) Marti-Renom, M. A.; Stuart, A.; Fiser, A.; Sánchez, R.; Melo, F.; Sali, A. Comparative Protein Structure Modeling of Genes and Genomes. *Annu. Rev. Biophys. Biomol. Struct.* **2000**, *29*, 291–325.

(53) Fiser, A.; Do, R. K.; Sali, A. Modeling of Loops in Protein Structures. *Protein Sci.* **2000**, *9*, 1753–1773.

(54) Arnold, K.; Bordoli, L.; Kopp, J.; Schwede, T. The SWISS-MODEL Workspace: a Web-based Environment for Protein Structure Homology Modelling. *Bioinformatics* **2006**, *22*, 195–201.

(55) Hess, B.; Kutzner, C.; van der Spoel, D.; Lindahl, E. GROMACS 4: Algorithms for Highly Efficient, Load-Balanced, and Scalable Molecular Simulation. *J. Chem. Theory Comput.* **2008**, *4*, 435–447.

(56) Oostenbrink, C.; Villa, A.; Mark, A. E.; van Gunsteren, W. F. A Biomolecular Force Field Based on the Free Enthalpy of Hydration and Solvation: The GROMOS Force-Field Parameter Sets 53A5 and 53A6. *J. Comput. Chem.* **2004**, *25*, 1656–1657.

(57) Berendsen, H. J. C.; Postma, J. P. M.; van Gunsteren, W. F.; Hermans, J. *Intermolecular Forces, Interaction Models for Water in Relation to Protein Hydration*; D. Reidel Publishing Co.: Dordrecht, The Netherlands, 1981.

(58) van der Spoel, D.; Lindahl, E.; Hess, B.; van Buuren, A. R.; Apol, E.; Meulenhobb, P. J.; Tieleman, D. P.; Sijbers, A. L. T. M.; Feenstra, K. A.; van Drunen, R.; Berendsen, H. J. C. *Gromacs User Manual*, version 4.0; Department of Biophysical Chemistry, University of Groningen: Groningen, The Netherlands, 2005; www.gromacs.org.

(59) Berendsen, H. J. C.; Postma, J. P. M.; van Gunsteren, W. F.; DiNola, A.; Haak, J. R. Molecular Dynamics with Coupling to an External Bath. *J. Chem. Phys.* **1984**, *81*, 3684–3690.

(60) Hess, B.; Bekker, H.; Berendsen, H. J. C.; Fraaije, J. G. E. M. LINCS: A Linear Constraint Solver for Molecular Simulations. *J. Comput. Chem.* **1997**, *18*, 1463–1472.

(61) Darden, T.; York, D.; Pedersen, L. G. Particle Mesh Ewald: An N-log(N) Method for Ewald Sums in Large Systems. *J. Chem. Phys.* **1993**, *98*, 10089–10092.

(62) Essmann, U.; Perera, L.; Berkowitz, M. L.; Darden, T.; Lee, H.; Pedersen, L. G. A Smooth Particle Mesh Ewald Method. *J. Chem. Phys.* **1995**, *103*, 8577–8593.

(63) Nosé, S. A Molecular Dynamics Method for Simulations in the Canonical Ensemble. *Mol. Phys.* **1984**, *52*, 255–268.

(64) Hoover, W. G. Canonical Dynamics: Equilibrium Phase-Space Distributions. *Phys. Rev. A* **1985**, *31*, 1695–1697.

(65) Parrinello, M.; Rahman, A. Polymorphic Transitions in Single Crystals: A New Molecular Dynamics Method. *J. Appl. Phys.* **1981**, *52*, 7182–7190.

(66) Nosé, S.; Klein, M. L. Constant Pressure Molecular Dynamics for Molecular Systems. *Mol. Phys.* **1983**, *50*, 1055–1076.

(67) http://www.arc.vt.edu/arc/SystemX/.

(68) Kabsch, W.; Sander, C. Dictionary of Protein Secondary Structure: Pattern Recognition of Hydrogen-Bonded and Geometrical Features. *Biopolymers* **1983**, *22*, 2577–2637.

(69) Turner, P. J. *Grace*; Center for Coastal and Land-Margin Research Oregon Graduate Institute of Science and Technology: Beaverton, OR, 2008.

(70) DeLano, W. L. *The PyMOL User's Manual*; DeLano Scientific: Palo Alto, CA, 2002.

(71) Pettersen, E. F.; Goddard, T. D.; Huang, C. C.; Greenblatt, D. M.; Meng, E. C.; Ferrin, T. E. UCSF Chimera—A Visualization System for Exploratory Research and Analysis. *J. Comput. Chem.* **2004**, *25*, 1605–1612.

(72) Abseher, R.; Horstink, L.; Hilbers, C. W.; Nilges, M. Essential Spaced Defined by NMR Structure Ensembles and Molecular Dynamics Simulation Show Significant Overlap. *Proteins* **1998**, *31*, 370–382.

(73) Philippopoulos, M.; Lim, C. Exploring the Dynamic Information Content of a Protein NMR Structure: Comparison of a Molecular Dynamics Simulation With the NMR and X-Ray Structures of *Escherichia coli* Ribonuclease HI. *Proteins* **1999**, *36*, 87–110.

(74) Dastidar, S. G.; Lane, D. P.; Verma, C. S. Multiple Peptide Conformations Five Rise to Similar Binding Affinities: Molecular Simulations of p53-MDM2. *J. Am. Chem. Soc.* **2008**, *130*, 13514–13515.

(75) Dastidar, S. G.; Lane, D. P.; Verma, C. S. Modulation of p53 Binding to MDM2: Computational Studies Reveal Important Roles of Tyr100. *BMC Bioinf.* **2009**, *10* (Suppl 15), S6.

(76) Dastidar, S. G.; Madhumalar, A.; Fuentes, G.; Lane, D. P.; Verma, C. S. Forces Mediating Protein-Protein Interactions: A Computational Stude of p53 "Approaching" MDM2. *Theor. Chem. Acc.* **2010**, *125*, 621–635.

(77) Shoemaker, B. A.; Portman, J. J.; Wolynes, P. G. Speeding Molecular Recognition by Using the Folding Funnel: The Fly-Casting Mechanism. *Proc. Natl. Acad. Sci. U.S.A.* **2000**, *97*, 8868–8873.

(78) Kuroki, R.; Kawakita, S.; Nakamura, H.; Yutani, K. Entropic Stabilization of a Mutant Human Lysozyme Induced by Calcium Binding. *Proc. Natl. Acad. Sci. U.S.A.* **1992**, *89*, 6803–6807.

(79) Young, L.; Post, C. B. Catalysis by Entropic Guidance from Enzymes. *Biochemistry* **1996**, *35*, 15129–15133.

(80) Yon, J. M.; Perahia, D.; Ghélis, C. Conformational Dynamics and Enzyme Activity. *Biochemie* **1998**, *80*, 33–42.

JP1011445